

Model-less Inversion-based Iterative Control for Output Tracking: Piezo Actuator Example [§]

Kyong-Soo Kim[†] Qingze Zou[‡]

Mechanical Engineering Department, Iowa State University, Ames, IA 50011

Abstract—In this article, we propose a model-less inversion-based iterative control (MIIC) approach for high-speed output tracking in repetitive applications such as the lateral scanning during atomic force microscope (AFM) imaging. The MIIC algorithm extends the inversion-based iterative control (IIC) technique and the enhanced inversion-based iterative control (EIIC) technique. The main contribution of this article is the development of the MIIC algorithm to eliminate the modeling process while further enhancing the output tracking performance. We explicitly consider the disturbance and/or measurement noise effect in the convergence analysis of the MIIC algorithm. It is shown that convergence can be reached in one iteration step if the noise/disturbance effect is negligible; Or, the input error can be quantified by the disturbance/noise to signal ratio (NSR, relative to the desired trajectory). The MIIC is applied to a piezo scanner on an atomic force microscope, and experimental results are presented to demonstrate the efficacy of the MIIC technique.

I. INTRODUCTION

In this paper, we propose a new model-less inversion-based iterative control (MIIC) technique for high-speed precision output tracking. It is noted that precision tracking of periodic trajectory at high-speed is needed in applications such as the nano-scale imaging/measurement using atomic force microscope (AFM) [1], the scanning mechanism on MEMS-based micro-mirrors [2], the quick-return mechanisms and cams in manufacturing, and the manufacturing process in rapid prototyping [3]. For example, in atomic force microscope (AFM) imaging, repetitive precision scanning at high-speed is needed to achieve high-speed imaging, which not only improves the throughput, but more importantly, enables the interrogation of nanoscale dynamic processes [1], [4]. It has been shown that iterative learning control (ILC) is quite efficient in tracking repetitive trajectories [5]. Limits, however, exist in conventional ILC designs [6] because causal controllers were used in these designs. As a result, the noncausality (i.e., the “preview” of the future desired trajectory as well as the output tracking of the system) was not exploited to improve the tracking, particularly for nonminimum-phase systems [6]. Such a limit is alleviated through the development of the IIC and the EIIC techniques. Although the IIC and the EIIC techniques utilize the noncausality to improve the tracking precision as illustrated in [7], their performance depends on the quality of the system dynamics model, whereas modeling process is time-consuming and prone to errors. The main contribution

of this paper is the development of the MIIC technique which eliminates the need for the dynamics model while further enhances the output tracking performance.

Iterative learning control approach [5] has been effective in the output tracking of repetitive operations. Compared to feedback control methods, the ILC approach avoids the potential stability issues caused by the high feedback gain (needed to achieve precision tracking). Instead, a learning mechanism is introduced in the ILC approach to utilize the repetitive nature of the applications to improve the tracking performance [8]. Moreover, ILC approach also has the advantages such as being ease to design and implement—as precision-model usually is not required in ILC algorithms. ILC techniques have been successfully implemented in various applications [9]. The majority of the ILC algorithms aims at obtaining a stable controller based on, for example, H_∞ robust control theory [10]. Such a stable controller, however, limits the ILC method in exploring the noncausality provided by the knowledge of the entire output tracking (not just at current time instant as in feedback control) through iterations. Particularly, we note that it has been shown recently [6] that a causal IIC controller is essentially equivalent to a feedback controller. Therefore, constraints exist in the conventional ILC approaches.

Such causality-related constraints in the ILC approaches are removed with the development of the inversion-based iterative control approach [11], [7], [12]. Particularly, the IIC approach utilizes the inverse of the system dynamics utilized a frequency-domain implementation scheme [7]. The convergence of the IIC algorithm, however, can be sensitive to the dynamic uncertainties of the system, i.e., the phase uncertainty of the system dynamics must be less $\pi/2$ to guarantee the convergence [7]. To improve the robustness of the IIC technique against the phase uncertainty, the enhanced inversion-based iterative control technique (EIIC) [12] was proposed. In the EIIC method, the updating of the input magnitude is decoupled from the updating of the input phase (in frequency-domain). As a result, the EIIC approach can achieve convergence in a larger frequency range at a faster convergence rate. The efficacy of the IIC and the EIIC algorithms have been demonstrated in experiments to achieve high-speed precision scanning, and to compensate for the cross-axis coupling-caused vibrations of piezotube actuators [7]. However, both the IIC and the EIIC algorithms require a reasonably-good model of the system dynamics, and the model accuracy determines the convergence rate (i.e., the choice of the iterative coefficient). We note that

[§] The work is supported by the NSF Grants CMMI-0626417 and DUE-0632908.

[†] E-mail: kyongsoo@iastate.edu.

[‡] Corresponding author, E-mail: qzzou@iastate.edu.

modeling of the system dynamics is time consuming and prone to errors, and the measured dynamics response heavily depends on the operation condition, which can also vary significantly from time to time (for example, for the probe positioning dynamics on AFM system). Therefore, there exist needs to overcome the modeling-related constraints in the IIC approach.

The main contribution of the article is the development of the MIIC technique. The MIIC algorithm does not require the modeling of the system dynamics, therefore, the constraints related to the modeling process, and the requirement for a good dynamics model are removed. Instead, the proposed MIIC algorithm updates the input-output relation of the system dynamics in each iteration by using the input-output signals measured in the previous iteration. We note that similar idea was utilized before in the adaptive ILC approaches in [13]. There exist, however, fundamental differences between the proposed MIIC technique and the adaptive ILC approaches as regard to how such online updating is utilized: In the adaptive ILC approaches [13], a dynamics model was used and the measured input-output signals were used to update the model; Whereas in the proposed method, no dynamics model is needed/used and the measured input-output signals were used to update the iterative control input directly. Moreover, we explicitly address the disturbance/noise effects—which was not considered in [13]—in the convergence analysis of the proposed MIIC algorithm. We show that the convergence of the MIIC algorithm can be achieved in one iteration when the noise/disturbance effect is negligible; Or, the input error can be quantified by the disturbance/noise to signal ratio (NSR, relative to the desired trajectory) when the disturbance and/or noise effects are not too large. The size of NSR for the MIIC algorithm to be effective (i.e., the tracking error is smaller when using the MIIC algorithm than that when not using it) is further quantified. We illustrate the proposed MIIC control technique by implementing it in experiments to the output tracking of a piezotube actuator on an AFM system. Two types of trajectories are used to evaluate the tracking performance with comparison to the IIC algorithm: triangular trajectories and band-limited white-noise type of trajectories. The experimental results show that precision output tracking is achieved in both cases, whereas the IIC algorithm failed to track the complicated band-limited white-noise trajectory. Moreover, the MIIC algorithm is also implemented to compensate for the hysteresis effect when tracking large-range triangle trajectory at high-speed. Experimental results indicate that precision output tracking can also be achieved.

II. MODEL-LESS INVERSION-BASED ITERATIVE CONTROL

We start with briefly reviewing the inversion-based iterative control [7] and the enhanced inversion-based iterative control [12] algorithm. These two control algorithms form the base for the proposed MIIC algorithm.

A. Inversion-based Iterative Control (IIC) and Enhanced Inversion-based Iterative control (EIIC)

IIC Algorithm [7] Recently, an inversion-based iterative control technique [7] was developed to achieve high-speed output tracking of periodic trajectories. For a stable, single input single output (SISO) system, the IIC control law can be described in the frequency-domain as

$$u_0(j\omega) = G_m(j\omega)^{-1}y_d(j\omega), \quad k = 0 \quad (1)$$

$$u_k(j\omega) = u_{k-1}(j\omega) + \rho(\omega)G_m(j\omega)^{-1}[y_d(j\omega) - y_{k-1}(j\omega)] \quad k \geq 1 \quad (2)$$

where ‘ $f(j\omega)$ ’ denotes the Fourier transform of the signal ‘ $f(t)$ ’, ‘ $y_d(\cdot)$ ’ denotes the desired output trajectory, ‘ $y_k(\cdot)$ ’ denotes the output obtained by applying the input ‘ $u_k(\cdot)$ ’ to the system during the k^{th} iteration, $\rho(\omega) > 0$ is the iterative coefficient, and $G_m(j\omega)$ denotes the frequency response model of the system. The convergence of the IIC algorithm is given in the following lemma 1.

Lemma 1: [7] At any given frequency ω , let both the actual dynamics of a SISO LTI system $G(j\omega)$ and its model $G_m(j\omega)$ be stable and hyperbolic (i.e., both have no zeros on the $j\omega$ axis), and the dynamics uncertainty $\Delta G(j\omega)$ be described as

$$\begin{aligned} \Delta G(j\omega) &= \frac{G(j\omega)}{G_m(j\omega)} = \frac{|G(j\omega)|e^{j\angle G(j\omega)}}{|G_m(j\omega)|e^{j\angle G_m(j\omega)}} \\ &\triangleq |\Delta G(\omega)|e^{j\Delta\angle G(j\omega)}, \end{aligned} \quad (3)$$

then the IIC control law converges at frequency ω to the desired input $u_d(j\omega) \triangleq G(j\omega)^{-1}y_d(j\omega)$, i.e., $\lim_{k \rightarrow \infty} u_k(j\omega) = u_d(j\omega)$, if and only if,

1) the iterative coefficient $\rho(\omega) \in \mathbb{R}$ is chosen as

$$0 < \rho(\omega) < \rho_{sup}(\omega) \triangleq \frac{2 \cos(\angle \Delta G(j\omega))}{|\Delta G(j\omega)|} \quad (4)$$

2) the magnitude of the phase variation is less than $\pi/2$, i.e.,

$$|\angle \Delta G(j\omega)| < \frac{\pi}{2} \quad (5)$$

EIIC Algorithm [12] The EIIC control law is also given in the frequency-domain as follows,

$$u_0(j\omega) = G_m(j\omega)^{-1}y_d(j\omega) \quad k = 0 \quad (6)$$

$$\begin{cases} |u_k(j\omega)| = |u_{k-1}(j\omega)| + \rho(\omega) |G_m^{-1}(j\omega)| [|y_d(j\omega)| - |y_{k-1}(j\omega)|] \\ \angle u_k(j\omega) = \angle u_{k-1}(j\omega) + (\angle(y_d(j\omega)) - \angle y_{k-1}(j\omega)) \end{cases} \quad k \geq 1$$

As shown in the above Eq. (6), the updating of the input magnitude is decoupled from the updating of the phase angle in the EIIC algorithm. As a result, the EIIC algorithm can converge in a larger frequency range and at a faster convergence rate than IIC algorithm, as given by the following Lemma 2.

Lemma 2: [12] For any given frequency value ω , let $G(j\omega)$, $G_m(j\omega)$ and $\Delta G(j\omega)$ be defined as in Lemma 1, respectively. Then the input of the EIIC law converges to the desired input $u_d(j\omega)$, i.e.,

$$\lim_{k \rightarrow \infty} |u_k(j\omega)| = |u_d(j\omega)|, \quad \text{and} \quad \lim_{k \rightarrow \infty} \angle u_k(j\omega) = \angle u_d(j\omega),$$

if and only if the iterative coefficient $\rho(\omega)$ is chosen as

$$0 < \rho(\omega) < \rho_{sup}(\omega) \triangleq \frac{2}{|\Delta G(j\omega)|} \quad (7)$$

The efficacy of the EIIC algorithm has been illustrated through experiments including the measurement of adhesion force measurement at high-speed using AFM [12], and the measurement of the time-dependent elastic modulus of a polymer material (Polydimethylsiloxane, PDMS) [14].

The implementation of the IIC and the EIIC algorithms, however, requires a reasonably good model of the system dynamics, while the modeling process can be time consuming and prone to errors. Thus, the success of the IIC and EIIC algorithms and the challenges involved in the dynamics modeling motivate the development of the following model-less inversion-based iterative control method.

B. Model-less Inversion-based Iterative Control (MIIC)

The proposed MIIC algorithm is given below:

$$u_0(j\omega) = \alpha y_d(j\omega), \quad (k=0),$$

$$u_k(j\omega) = \begin{cases} \frac{u_{k-1}(j\omega)}{y_{k-1}(j\omega)} y_d(j\omega), & (k \geq 1), \\ 0 & \text{when } y_k(j\omega) \neq 0 \text{ and } y_d(j\omega) \neq 0 \\ & \text{otherwise} \end{cases}$$

where $\alpha \neq 0$ is a pre-chosen constant (e.g., α can be chosen as the estimated DC-Gain of the system). Next, we discuss the convergence of the MIIC algorithm upon the additional disturbance and/or measurement noise effect.

Theorem 1: Let $G(j\omega)$ be a stable SISO LTI system, then at frequency ω ,

- 1) if the disturbance (and/or noise) effects are negligible, then convergence is reached after one iteration, i.e.,

$$u_1(j\omega) = u_d(j\omega), \quad (8)$$

- 2) if the system output $y(j\omega)$ is effected by the disturbance and/or the measurement noise as

$$y(j\omega) = y_l(j\omega) + y_n(j\omega), \quad (9)$$

where $y_l(j\omega)$ denotes the linear part of the system response to the input $u(j\omega)$, i.e. $y_l(j\omega) = G(j\omega)u(j\omega)$, and $y_n(j\omega)$ denotes the output component caused by disturbances and/or measurement noise. Then at the k^{th} iteration, the ratio of the iterative control input to the desired input is given by:

$$\frac{u_k(j\omega)}{u_d(j\omega)} = \frac{G(j\omega)}{G(j\omega)(1+S_k(j\omega))+P_k(j\omega)/\alpha}, \quad \forall k \geq 1 \quad (10)$$

where $P_k(j\omega)$ denotes the product of the noise/disturbance-to-signal (NSR) ratios (relative to the desired output $y_d(j\omega)$) at frequency ω from all the past iterations, and $S_k(j\omega)$ denotes the summation of the product $P_k(j\omega)$,

$$P_k(j\omega) = \prod_{i=0}^{k-1} \frac{y_{i,n}(j\omega)}{y_d(j\omega)},$$

$$S_k(j\omega) = \begin{cases} 0, & \text{for } k=1 \\ \sum_{j=1}^{k-1} \prod_{i=1}^j \frac{y_{k-i,n}(j\omega)}{y_d(j\omega)}, & \text{for } k \geq 2 \end{cases}$$

Theorem 2: Let assumptions in Theorem 1 be satisfied,

- 1) assume that during each iteration, the NSR is bounded above by a positive, less-than-half constant $\varepsilon(\omega)$, i.e.,

$$\left| \frac{y_{k,n}(j\omega)}{y_d(j\omega)} \right| \leq \varepsilon(\omega) < 1/2, \quad \forall k \quad (11)$$

then the ratio of the iterative input to the desired input is bounded in magnitude and phase, respectively, as

$$R_{\min}(\omega) \triangleq 1 - \varepsilon(\omega) \leq \lim_{k \rightarrow \infty} \left| \frac{u_k(j\omega)}{u_d(j\omega)} \right|$$

$$\lim_{k \rightarrow \infty} \left| \frac{u_k(j\omega)}{u_d(j\omega)} \right| \leq \frac{1 - \varepsilon(\omega)}{1 - 2\varepsilon(\omega)} \triangleq R_{\max}(\omega)$$

$$\lim_{k \rightarrow \infty} \left| \angle \left(\frac{u_k(j\omega)}{u_d(j\omega)} \right) \right| \leq \sin^{-1} \left(\frac{\varepsilon(\omega)}{1 - \varepsilon(\omega)} \right) \triangleq \theta_{\max}(\omega),$$

and the relative tracking error is bounded as

$$\lim_{k \rightarrow \infty} \left| \frac{y_k(j\omega) - y_d(j\omega)}{y_d(j\omega)} \right| \leq \frac{2\varepsilon(\omega)(1 - \varepsilon(\omega))}{1 - 2\varepsilon(\omega)} \quad (12)$$

- 2) The use of the MIIC algorithm will improve the tracking at frequency ω , i.e.,

$$\lim_{k \rightarrow \infty} \left| \frac{y_k(j\omega) - y_d(j\omega)}{y_d(j\omega)} \right| < 1, \quad (13)$$

if the NSR is bounded above by $1 - \frac{\sqrt{2}}{2}$, i.e.,

$$\left| \frac{y_{k,n}(j\omega)}{y_d(j\omega)} \right| \leq \varepsilon(\omega) < 1 - \frac{\sqrt{2}}{2}, \quad \forall k \quad (14)$$

Remark 1: Theorem 2 implies that precision tracking at frequency ω can be achieved provided that the NSR at that frequency is small, which agrees with our intuition. Additionally, Theorem 2 gives a guideline to determine the frequency range over which the MIIC law can be applied in practices (Eq. (14)).

III. EXPERIMENTAL EXAMPLE: PIEZO ACTUATOR OUTPUT TRACKING

In this section, we illustrate the MIIC technique by implementing it to the output tracking of a piezotube actuator on an AFM system. We start with describing the experimental system next.

A. Experimental setup

The schematic diagram of the experimental AFM system (Dimension 3100, Veeco Inc.) is shown in Fig. 1 for the control of the x-axis piezotube actuator. All the control inputs to the piezo actuator were generated by using MATLAB-xPC-target package, and sent out through a data acquisition card (DAQ) to drive the piezo actuator via an amplifier—The AFM-controller had been customized so that the PID control circuit was bypassed when the external control input was applied.

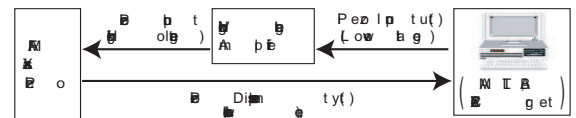


Fig. 1. Schematic diagram of the experiment setup to implement the proposed MIIC algorithm.

B. Implementation and Tracking Results

Output Tracking of Triangle Trajectory We note that triangle trajectories are commonly used in many scanning operations such as the AFM imaging. The displacement range was chosen small ($5\mu\text{m}$, $\sim 5\%$ of the total displacement range of the piezotube actuator), thereby the effect of the nonlinear hysteresis became small and negligible (as hysteresis effect is range-dependent) [7]. Three different rates (2Hz, 100Hz and 300Hz) of the triangle trajectory were chosen—which correspond to the tracking in the slow, medium and fast speed ranges (relative to the bandwidth of the piezo actuator), respectively. The tracking results are shown in Fig. 2, with comparison to those obtained by using the IIC technique. The readers are referred to Ref. [15] for the details of the IIC algorithm implementation. Moreover, the experimental tracking results are also compared quantitatively in Table. I in terms of the relative maximum error $E_{\max}(\%)$ and the relative root mean square (RMS) error $E_{\text{rms}}(\%)$, defined as below

$$E_{\max}(\%) \triangleq \frac{\|y_d(\cdot) - y(\cdot)\|_{\infty}}{\|y_d(\cdot)\|_{\infty}} \times 100, \quad E_{\text{rms}}(\%) \triangleq \frac{\|y_d(\cdot) - y(\cdot)\|_2}{\|y_d(\cdot)\|_2} \times 100. \quad (15)$$

In the experiments, we stopped the iterations of the MIIC law (or the IIC law) when neither one of the above two errors, $E_{\max}(\%)$ or $E_{\text{rms}}(\%)$, can be further reduced. The iterative input for tracking multiple (over 10) periods of triangles was sent to the system, and the averaged results are shown in Table. I and Fig. 2 (The un-averaged results are compared with the averaged ones later). Also, the iteration numbers used in the experiments are listed in Table I.

Output Tracking of a Band-limited White-Noise Type of Trajectory We note that the triangle trajectory only consists of a few significant frequency components (i.e., multiple integer times of the fundamental frequency of the triangle signal), whereas a band-limited white-noise type of trajectory has much richer frequency components—up to the cut-off frequency. Therefore, it is more challenging to track band-limited white noise type of trajectories than to track triangle trajectories. Specifically, the band-limited white-noise of one second duration and three different cut-off frequencies, 400 Hz, 800 Hz, and 1050 Hz, were generated by using MATLAB, and then duplicated for multiple copies to form the desired trajectory. The maximum displacement of the desired trajectory was limited within $1.5\mu\text{m}$. The tracking errors are shown in Table II. For comparison, the IIC algorithm was also implemented to track the three chosen white-noise type of trajectories. The obtained output tracking results are compared in Fig. 3.

Output Tracking of Large-range Triangle Trajectory The proposed MIIC technique was also applied to track large-range triangle trajectories to evaluate its efficacy in compensating for the nonlinear hysteresis effect. To demonstrate the amount of the tracking error caused by the hysteresis and vibration dynamics effects, the output tracking with the DC gain method was obtained, where neither the hysteresis nor the vibrational dynamics effect was compen-

sated for, i.e., the input was obtained by simply scaling the desired output with the DC gain of the system. It is noted that the hysteresis effect of piezo actuators is significant as the displacement range becomes large. The triangle trajectories with the displacement range of $50\mu\text{m}$ was chosen. Such a displacement range is over 60% of the full displacement range of the piezotube actuator, and the hysteresis effect became pronounced in the output tracking. The tracking results are shown in Fig. 4 and Table. III.

C. Discussion of the Experiment Results

Triangle trajectory tracking The tracking results in Table. I show that by using the proposed MIIC algorithm, precision output tracking can be achieved. For the triangle trajectories at 2 Hz and 100 Hz, the tracking errors obtained by using the MIIC algorithm are similar to the error when the IIC method was used (see Fig. 2). However, only two iterations were needed for MIIC law to reach convergence, compared to 3 to 4 iterations needed for the IIC law. As the triangle rate increased to 300 Hz, the tracking error obtained by using the MIIC algorithm was 7 times smaller than the error by using the IIC algorithm (see Table I). Note the frequency range to implement the MIIC (or IIC) algorithm is a design parameter, and the frequency range was chosen as 2.5 KHz and 1 KHz for the MIIC algorithm and the IIC algorithm, respectively, to optimize the tracking results. Particularly, we notice that divergence occurred if the frequency range was chosen larger than 1.4 KHz for the IIC algorithm. This can be explained by using the frequency response of the system: large phase variation exists for frequencies larger than 1 KHz, which becomes larger than $\pi/2$ around the second resonant peak at 1.3KHz. Therefore, by Lemma 1, the output tracking will diverge at those frequencies. On the contrary, the proposed MIIC algorithm is not limited by such phase uncertainties, thereby the tracking performance can be further improved (see Fig. 2 (a3), (b3)). Moreover, we compared the power spectrum (estimated by using MATLAB) of the tracking error with that of the desired trajectory. It was found that the maximum power spectrum value of the tracking error was only less than 0.4% of that of the desired trajectory. This implies that the change of the iterative control input to further decrease the tracking error became close to the noise level of the system. Thus, the experimental results show the superior tracking performance of the MIIC algorithm over the IIC algorithm.

Band-limited white-noise tracking The band-limited white noise type of tracking trajectory has much richer frequency components than the triangle trajectory, which is evident as revealed by the power spectrum of the three band-limited white noise trajectories shown in Fig. 3(c1). The experimental results (Table. II and Fig. 3 show that by using the MIIC technique, precision output tracking can still be achieved for such complex trajectories. For band-limited white-noise trajectory with the cut-off frequency of 400 Hz, the tracking errors obtained by using the MIIC technique

TABLE I

PERFORMANCE COMPARISON OF THE MIIC ALGORITHM AND THE IIC ALGORITHM FOR TRACKING THE TRIANGLE TRAJECTORY AT THREE DIFFERENT TRIANGLE RATES, WHERE $E_{rms}(\%)$ AND $E_{max}(\%)$ ARE DEFINED IN EQ. (15), AND THE ITERATION NUMBERS USED ARE ALSO LISTED. THE DISPLACEMENT RANGE IS $5 \mu\text{m}$.

| Iter. No. | $E_{rms}(\%)$ | | | | | | $E_{max}(\%)$ | | | | | |
|-----------|---------------|---------|--------|--------|--------|---------|---------------|--------|--------|--------|--------|---------|
| | 2 Hz | | 100 Hz | | 300 Hz | | 2 Hz | | 100 Hz | | 300 Hz | |
| | MIIC | IIC | MIIC | IIC | MIIC | IIC | MIIC | IIC | MIIC | IIC | MIIC | IIC |
| 1 | 0.6026 | 1.3529 | 0.7160 | 4.5145 | 2.0689 | 12.7279 | 1.1106 | 1.5927 | 1.7450 | 4.7731 | 5.8387 | 17.7013 |
| 2 | 0.2291 | 0.3033 | 0.3477 | 3.0220 | 1.7508 | 12.1486 | 0.7296 | 0.9274 | 1.5784 | 4.9721 | 5.4809 | 19.7839 |
| 3 | 0.2279 | 0.2338 | 0.3243 | 2.5296 | 1.7529 | 12.1497 | 0.7890 | 0.9197 | 1.6046 | 5.3670 | 5.4594 | 19.3573 |
| 4 | 0.2292 | 0.23256 | 0.3267 | 2.0518 | 1.7517 | 12.1394 | 0.7677 | 0.6804 | 1.6598 | 2.6577 | 5.5369 | 19.4687 |

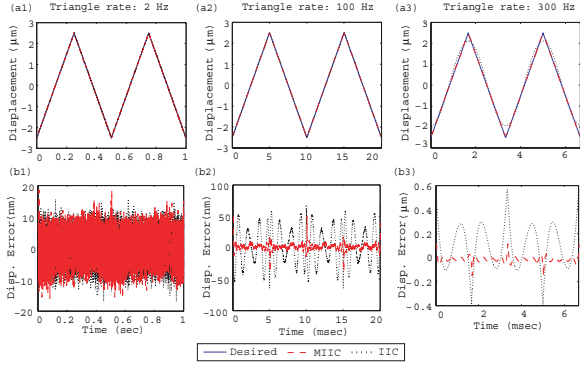


Fig. 2. Experimental results: (top row) comparison of the output tracking obtained by using the MIIC algorithm with the tracking by the IIC algorithm for three different triangle rates; and (bottom row) comparison of the corresponding tracking errors.

were very small (the relative RMS error is less than 2%). Such tracking precision was maintained even when the cut-off frequency became much higher (800 Hz and 1.05 KHz). We note that to achieve the same tracking precision (RMS error $E_{rms} \leq 2\%$) by using feedback control approaches, the closed-loop sensitivity $S(j\omega)$ must be below -34 dB (i.e., 0.02) for frequency $\omega \leq 1.05 \text{ KHz}$, which, in turn, requires the closed-loop bandwidth to be much higher than the cut-off frequency of 1.05 KHz. Such high bandwidth is extremely difficult to achieve with feedback control—if not entirely impossible, as the cut-off frequency of 1.05 KHz is well beyond the bandwidth of the piezo actuator to encompass two resonant peaks as well as one “dip” (i.e., highly under-damped zero) of the piezo actuator dynamics. Note that such a comparison is to highlight the efficacy of the proposed MIIC algorithm in achieving output tracking of broad-band trajectories in repetitive operations, in the light of the Result of Ref. [6] that an equivalent feedback controller exists for causal iterative learning algorithms. The experimental results also show that the proposed MIIC technique is robust against system dynamics uncertainty, particularly the phase uncertainty. As we can see from Fig. 3, divergences occurred when the IIC method was used to track such complex broad-band trajectories. For the band-limited white-noise trajectory with cut-off frequency of 400 Hz, large tracking error occurred, which became much larger than the desired trajectory itself as the cut-off frequency increased to 800 Hz and 1.05 KHz. This is because the IIC method is more sensitive to the model uncertainty, particularly the phase uncertainty. Such sensitivity of the iteration to the phase uncertainty is removed in the MIIC

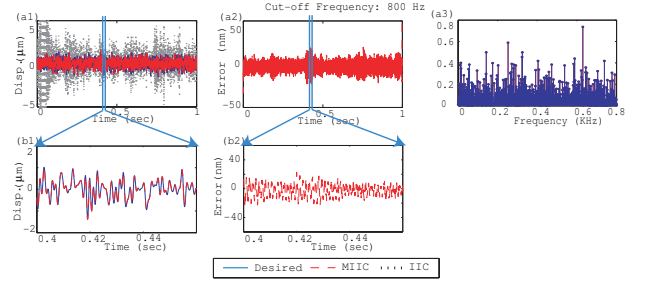


Fig. 3. Comparison of the tracking results the band-limited white-noise trajectory at cut-off frequency of 800 Hz by using the MIIC algorithm with those obtained by using the IIC algorithm (a1), the corresponding tracking errors by using the MIIC algorithm (a2), zoom in plots (b1, b2) and the power spectrum of the band-limited white noise desired trajectory (blue circle) with the power spectrum of the output tracking obtained by using the MIIC algorithm (red cross) (c1).

technique. Therefore, the experimental results show that the proposed MIIC algorithm is superior to other iterative control algorithms like the IIC method in high-speed tracking of complex desired trajectories.

Large-range triangle trajectory The tracking results in Table. III and Fig. 4 show that precision tracking at large displacement range can also be achieved by using the MIIC algorithm. As revealed by the output tracking obtained by using the DC-gain method, the hysteresis effect became pronounced at such large displacement range ($50 \mu\text{m}$, Fig. 4 (a)), which was augmented with the vibrational dynamics effects at high-speed (100 Hz and 300 Hz), resulting in larger tracking errors, see Fig. 4 (b), (c). The experimental results show that at slow-speed (2 Hz) tracking, the tracking error obtained by the MIIC algorithm was small (the relative RMS error and the relative maximum error are at 0.22 % and 0.37 %, respectively). Such a tracking precision is very close to that of tracking small range triangle trajectory (Compare Table I with Table II). Even at much higher speeds (100 Hz and 300 Hz), precision-tracking was still maintained. For example, the relative RMS error was still only about 4.7 % for tracking the triangle trajectory of 300 Hz. We note that such an error is slightly larger than the error for small range tracking. This is mainly due to the reduction of the frequency range over which the MIIC algorithm was used (from 2.5 KHz to 2 KHz—to prevent the input voltage from saturation). Also Table III shows that more iterations were needed for large-range tracking than those for the small-range tracking. This is because at large-range tracking, the dynamics variations caused by the hysteresis effect became pronounce. Therefore, the

TABLE II

TRACKING PERFORMANCE COMPARISON OF THE MIIC WITH THE IIC ALGORITHMS TO TRACK A BAND-LIMITED WHITE NOISE TRAJECTORY WITH DIFFERENT CUT-OFF FREQUENCIES ARE WHERE “ITER. NO.” DENOTES THE NUMBER OF ITERATIONS USED IN EXPERIMENTS.

| Iter. No. | E_{rms} (%) | | | | | | E_{max} (%) | | | | | |
|-----------|---------------|---------|--------|----------|---------|----------|---------------|---------|--------|----------|---------|---------|
| | 400 Hz | | 800 Hz | | 1050 Hz | | 400 Hz | | 800 Hz | | 1050 Hz | |
| | MIIC | IIC | MIIC | IIC | MIIC | IIC | MIIC | IIC | MIIC | IIC | MIIC | IIC |
| 1 | 2.6123 | 17.1439 | 4.5240 | 94.1437 | 4.93406 | 962.8028 | 3.3647 | 17.3808 | 5.7165 | 98.9275 | 6.7249 | 1003.9 |
| 2 | 1.5548 | 63.2610 | 1.3014 | 350.1737 | 1.2710 | Diverge | 1.9774 | 61.4206 | 4.5881 | 563.5381 | 3.1347 | Diverge |
| 3 | 1.5060 | Diverge | 1.3223 | Diverge | 1.1992 | Diverge | 2.0713 | Diverge | 4.9661 | Diverge | 3.3160 | Diverge |
| 4 | 1.7034 | Diverge | 1.3355 | Diverge | 1.1934 | Diverge | 2.3516 | Diverge | 4.9499 | Diverge | 3.1175 | Diverge |

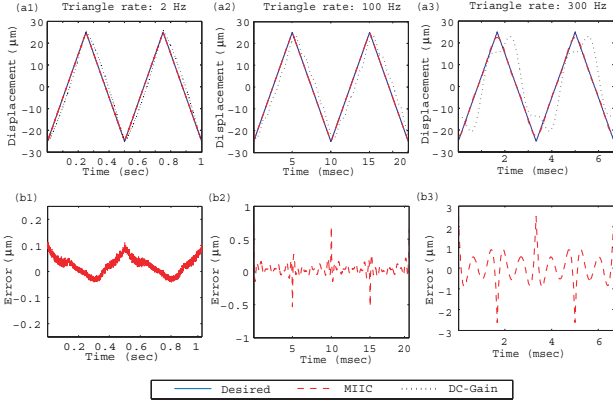


Fig. 4. (top row) Comparison of the output tracking obtained by using the DC-Gain method with the tracking by the MIIC algorithm at the rates of (a1) 2 Hz, (a2) 100 Hz and (a3) 300 Hz, and (bottom row) the corresponding tracking errors obtained by using the MIIC algorithm.

TABLE III

TRACKING PERFORMANCE ACHIEVED BY USING THE MIIC ALGORITHM TO TRACK A LARGE RANGE TRIANGULAR TRAJECTORY AT DIFFERENT SPEEDS. THE NUMBER OF ITERATIONS (ITER. NO.) USED IS ALSO LISTED.

| Iter. No. | E_{rms} (%) | | | E_{max} (%) | | |
|-----------|---------------|--------|--------|---------------|--------|--------|
| | 2 Hz | 100 Hz | 300 Hz | 2 Hz | 100 Hz | 300 Hz |
| 1 | 16.28 | 14.92 | 16.78 | 17.87 | 14.48 | 17.50 |
| 2 | 5.83 | 4.45 | 6.43 | 6.05 | 4.84 | 8.51 |
| 3 | 2.02 | 1.58 | 4.87 | 2.04 | 4.01 | 11.16 |
| 4 | 0.61 | 0.84 | 4.76 | 0.74 | 1.57 | 10.43 |
| 5 | 0.22 | 0.61 | 4.75 | 0.38 | 2.46 | 10.48 |

experimental results demonstrate that the MIIC algorithm can be used to compensate for both the hysteresis and dynamics effects simultaneously.

IV. CONCLUSIONS

This article introduced a model-less inversion-based iterative control for tracking of repetitive trajectories at high-speed. The convergence of the MIIC algorithm was analyzed for both the case when the noise/disturbance is negligible and the case when the effect of the disturbance/noise is considered. It was shown that the convergence can be achieved in one-step iteration when the noise effect is negligible. When the disturbance/noise effect is considered, the input error at a given frequency, as measured by the ratio of the iterative input to the desired input, was quantified in terms of the disturbance/noise to signal ratio (relative to the desired trajectory). It was shown that the convergence of the MIIC algorithm can be guaranteed when the NSR is smaller than one-half, and the MIIC algorithm will improve the tracking if the NSR is less than $1 - 1/\sqrt{2}$. The proposed method was applied to the output tracking of a piezo actuator on an

Atomic Force Microscope (AFM). The experimental results demonstrated that the MIIC can achieve precision output tracking for both high-speed triangle trajectories and band-limited white-noise type of trajectories with cut-off frequency beyond the bandwidth of the piezo actuator. Moreover, precision output tracking of a large-size triangle trajectory at high-speed can also be achieved, indicating the ability of the proposed approach to compensate for the hysteresis effect simultaneously.

REFERENCES

- [1] R. Wiesendanger, ed., *Scanning Probe Microscopy and Spectroscopy*. Cambridge University Press, 1994.
- [2] F. Filhol, E. Defay, C. Divoux, C. Zinck, and M. Delaye, “Resonant micro-mirror excited by a thin-film piezoelectric actuator for fast optical beam scanning,” *SENSORS AND ACTUATORS A-PHYSICAL*, vol. 123, pp. 483–489, 2005.
- [3] S. Huang and W. Shen, “Development of a multi-optical source rapid prototyping system,” *INTERNATIONAL JOURNAL OF ADVANCED MANUFACTURING TECHNOLOGY*, vol. 27, no. 1, 2005.
- [4] F. Zimmer, H. Grueger, A. Heberer, T. Sandner, A. Wolter, and H. Schenk, “Scanning micro-mirrors: From bar-code-scanning to spectroscopy,” in *OPTICAL SCANNING* (S. Sagan and G. Marshall, eds.), vol. 5873 of *Proceedings of SPIE*, pp. 84–94, 2005.
- [5] L. Moore, K. and J.-X. E. Xu, “Special issue on iterative learning control, int. journal of control,” Vol. 73(10) 2000.
- [6] M. Verwoerda, G. Meinsma, and T. de Vries, “On admissible pairs and equivalent feedback-youla parameterization in iterative learning control,” *Automatica*, vol. 42, pp. 2079 – 2089, 2006.
- [7] S. Tien, Q. Zou, and S. Devasia, “Iterative control of dynamics-coupling-caused errors in piezoscanners during high-speed afm operation for high-speed afm operation,” *IEEE Trans. on Control Systems Technology*, vol. 13, no. 6, pp. 921–931, 2005.
- [8] Q. Zou, K. K. Leang, E. Sadoun, M. J. Reed, and S. Devasia, “Control issues in high-speed afm for biological applications: Collagen imaging example,” *Special Issue on “Advances in Nano-technology Control”*, *Asian Journal Control*, vol. 8, pp. 164–178, June 2004.
- [9] C. Cloet, M. Tomizuka, and R. Horowitz, “Design requirements and reference trajectory generation for a copier paper-path,” in *IEEE/ASME International Conference on Advanced Intelligent Mechatronics Proceedings*, (Como, Italy), pp. 911–916, July 2001.
- [10] P. Gaspar and J. Bokor, “Iterative model-based mixed h_2 / h_{∞} control design,” ’98. *UKACC International Conference*, vol. 1, pp. 1–4, 1998.
- [11] J. Ghosh and B. Paden, “A pseudoinverse-based iterative learning control,” May 2002.
- [12] K.-S. Kim, Q. Zou, and C. Su, “Iteration-based scan-trajectory design and control with output-oscillation minimization: Atomic force microscope example,” *American Control Conference*, 2007.
- [13] K. L. Moor, M. Dahleh, and S. P. Bhattacharyya, “Iterative learning control: A survey and new results,” *Journal of Robotic Systems*, vol. 9, pp. 563–594, 1992.
- [14] K.-S. Kim, Z. Lin, P. Shrotriya, and S. Sundararajan, “Iterative control approach to high-speed force-distance curve measurement using afm: Time dependent response of PDMS,” *UltraMicroscopy*, 2007. Submitted.
- [15] Q. Zou and Y. Wu, “Iterative control approach to compensate for both the hysteresis and the dynamics effect of piezo actuators,” *IEEE Trans. on Control Systems Technology*, vol. 15, 2007.